

Supplemental material: Numerical study on the mechanism of drag modulation by dispersed drops in two-phase Taylor-Couette turbulence

Jinghong Su,¹ Lei Yi,¹ Bidan Zhao,² Cheng Wang,¹ Fan Xu,² Junwu Wang,² and Chao Sun^{1,3}

¹*New Cornerstone Science Laboratory, Center for Combustion Energy,
Key Laboratory for Thermal Science and Power Engineering of Ministry of Education,
Department of Energy and Power Engineering, Tsinghua University, 100084 Beijing, China*

²*State Key Laboratory of Multiphase Complex Systems, Institute of Process Engineering,
Chinese Academy of Sciences, P. O. Box 353, Beijing 100190, PR China*

³*Department of Engineering Mechanics, School of Aerospace Engineering, Tsinghua University, Beijing 100084, China*

NUMERICAL METHODS AND COMPUTATIONAL ACCURACY

The simulations are performed using a volume-of-fluid (VOF) method with a piecewise-linear interface calculation (PLIC) algorithm, which is implemented in the interFoam solver of the open-source OpenFOAM v8. In the VOF method, the phase fraction variable α is utilized in each cell to characterize the distribution of the two phases. The range of α is from zero to one, where $\alpha = 0$ represents the continuous phase, $\alpha = 1$ represents the dispersed phase, and $0 < \alpha < 1$ represents the interface region. The evolution of α is governed by the transport equation

$$\partial_t \alpha + \nabla \cdot (\alpha \mathbf{u}) = 0, \quad (\text{S1})$$

where \mathbf{u} is the velocity field. Because of the continuity of the phase fraction, the interface between the two phases tends to become smeared. To mitigate this issue, previous versions of OpenFOAM implemented an interface compression approach based on the counter-gradient transport to keep the sharpness of the interface [1]. In addition, the multidimensional universal limiter with explicit solution (MULES) algorithm is implemented to ensure that the phase fraction α remains within the strict bounds of 0 and 1. After adding the interface compression term which is only

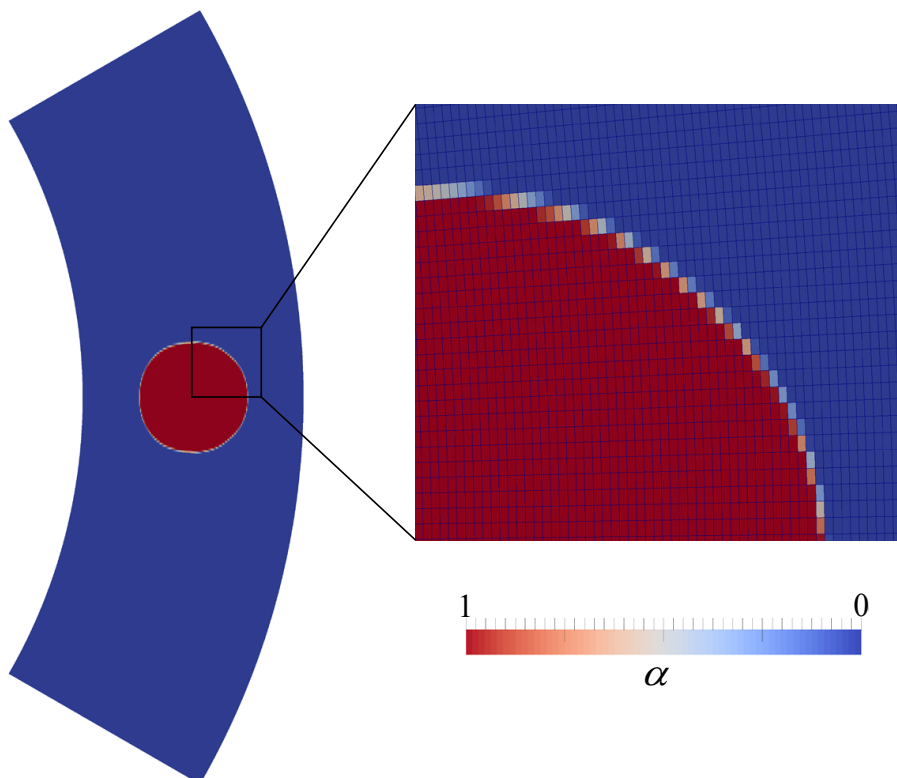


FIG. S1: A snapshot of the two-phase interface resolved by the PLIC algorithm.

active at the interface, the transport equation becomes

$$\partial_t \alpha + \nabla \cdot (\alpha \mathbf{u}) + \nabla \cdot [\alpha(1 - \alpha) \mathbf{u}_c] = 0, \quad (\text{S2})$$

where $\mathbf{u}_c = c \mathbf{u} \nabla \alpha / |\nabla \alpha|$ with c being the compression factor. Alternatively, a PLIC-based algorithm has been recently implemented to capture the interface more accurately. This algorithm involves representing the interface between the two phases by employing surface-cuts which split each cell to match the volume fraction of the phase in that cell. The surface-cuts are oriented according to the point field of the local phase fraction. The phase fraction on each cell face is then calculated from the amount submerged below the surface-cut. Note that this algorithm may not handle certain cells when the cut position is unclear or multiple interfaces exist. In such cases, the interface compression approach is still applied to those cells. Compared to the traditional PLIC method, the present approach is easier to implement when using an unstructured mesh. Moreover, when solving practical engineering problems, the combination of the present method with the interface compression approach enhances the robustness of the solutions. Therefore, we have employed this PLIC-based VOF method in our study to deal with the two-phase turbulence in TC system. Figure S1 shows a snapshot of a droplet placed in the Taylor-Couette system. The resolved interface region ($0 < \alpha < 1$) is confined within a single layer of grid cells between the two phases to ensure sharpness of the interface.

Spurious currents have long been a significant obstacle in relevant research, affected by factors including surface tension coefficient, grid resolution, time step, density ratio, and viscosity ratio between phases [2–4]. To date, completely eliminating spurious currents remains a formidable challenge. In our study, we address this issue by carefully selecting suitable simulation conditions and parameters to ensure that spurious currents remain within an acceptable range. Figure S2 shows a snapshot of a static drop with a diameter half of the gap width. The density ratio of the drop to the continuous phase is set as 1/4 and the viscosity ratio is set as 1/4 which has strongest spurious currents considered in our work. The inner and outer cylinders are fixed and the spurious current mainly appear near the two-phase interface. The normalized maximum velocity magnitude is limited to below 1.8% as shown in Fig. S2. By doing this, the almost constant conserved quantity for two-phase flow could be obtained as shown by the black solid line in Fig. S3. The ratio of the fluctuation and mean value of the conserved quantity is below 1.2%.

The schemes of the time integration and spatial discretization are listed below. We utilize a blended scheme for the temporal term discretization, which lies between the first-order Euler scheme and the second-order Crank-Nicolson scheme. To ensure robustness and accuracy, we set the blending factor to 0.9. For spatial discretization, we employ a second-order linear-upwind scheme to discretize the advection term in the momentum equation. The phase fraction transport equation is solved using a piecewise-linear interface calculation (PLIC) scheme. The pressure-velocity coupling is handled using the PIMPLE algorithm. The pressure equation is solved using the Geometric Algebraic

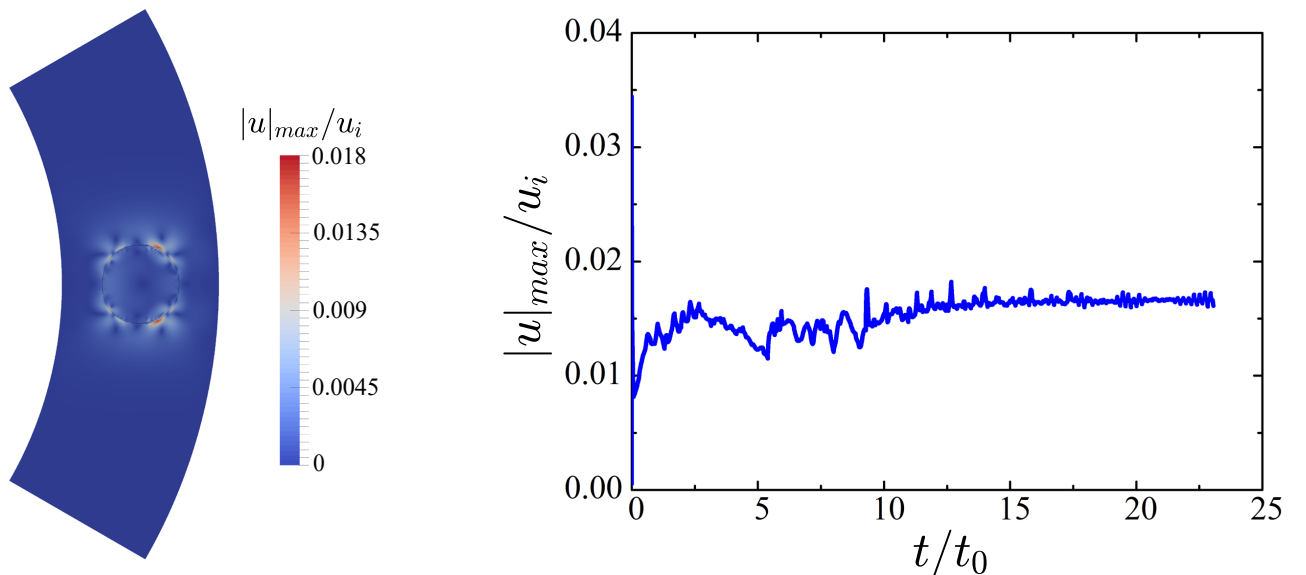


FIG. S2: Spurious currents for a static drop in a Taylor-Couette system with the two cylinders fixed. (a) Contour of the velocity magnitude. (b) The maximum velocity magnitude as a function of time. The maximum velocity magnitude is normalized by the velocity of the inner cylinder u_i considered in our work and the time t is normalized by the time required for one turn of the inner cylinder $t_0 = 2\pi r_i / u_i$, where r_i is the radius of the inner cylinder.

Multigrid (GAMG) solver coupled with the Simplified Diagonal-based Incomplete Cholesky (DIC) smoother. For solving velocity and phase fraction, we use an iterative solver with a symmetric Gauss-Seidel smoother. In the simulation, we maintain a tolerance of 10^{-6} for all variables to control the residuals, except for the phase fraction, which has a tolerance of 10^{-8} .

We have before performed simulations using OpenFOAM for single-phase flows with a range of Taylor number from $Ta = 5.84 \times 10^3$ to $Ta = 2.39 \times 10^7$ with the temporal term discretized using a second-order implicit backward inferencing scheme [5, 6] and validated our results through comparisons with those from Ostilla et al. [7]. Considering our temporal term is discretized with a blended scheme, we have additionally simulated two cases with the Taylor number being $Ta = 3.90 \times 10^6$ (Re = 1600) and $Ta = 9.52 \times 10^6$ (Re = 2500) and compared our results with those from Ostilla et al [7], as shown in Table 1. In our work, the minimum flow geometry with a rotational symmetry of six ($n_{sym} = 6$, i.e., the azimuthal angle of the simulated domain is $\pi/3$) and an aspect ratio of $\Gamma = L/d = 2\pi/3$ is selected to reduce the computational cost while not affecting the results, which has been verified by previous studies [8, 9]. The L denotes the axial length and d denotes the gap width. Regarding the deviation analysis, we represent the Nusselt number Nu_ω from Ostilla et al. [7] and OpenFOAM as $Nu_{\omega, Ot}$ and $Nu_{\omega, Op}$, respectively. The deviation is obtained by $Nu_{\omega, Op}/Nu_{\omega, Ot} - 1$ at the same Reynolds number. A deviation of +1.13% is found at Re=1600 and a deviation of -1.37% is found at Re = 2500, indicating that the chosen time scheme is sufficient to capture the flow field information.

	Re	Ta	n_{sym}	Γ	$N_\theta \times N_r \times N_z$	Nu_ω	Deviation
Ostilla et al.	1600	3.90×10^6	1	2π	$300 \times 144 \times 144$	5.42553	—
OpenFOAM	1600	3.90×10^6	6	$2\pi/3$	$80 \times 160 \times 80$	5.48683	+1.13%
Ostilla et al.	2500	9.52×10^6	1	2π	$384 \times 192 \times 192$	6.42160	—
OpenFOAM	2500	9.52×10^6	6	$2\pi/3$	$100 \times 192 \times 100$	6.33191	-1.37%

TABLE I: Validity of the calculation results for the single-phase flow at Re = 1600 and Re = 2500.

FORMULA DERIVATION OF THE CONSTANT AZIMUTHAL MOMENTUM TRANSPORT

The azimuthal momentum in a Taylor-Couette flow in the cylindrical coordinate system (r, θ, z) is governed by

$$\begin{aligned} \frac{\partial(\rho u_\theta)}{\partial t} + \frac{2\rho u_r u_\theta}{r} + \frac{\partial(\rho u_r u_\theta)}{\partial r} + \frac{1}{r} \frac{\partial(\rho u_\theta u_\theta)}{\partial \theta} + \frac{\partial(\rho u_\theta u_z)}{\partial z} &= \frac{2}{r} \left(\frac{\mu}{r} \frac{\partial u_r}{\partial \theta} + \frac{\mu \partial u_\theta}{\partial r} - \frac{\mu u_\theta}{r} \right) + \\ \frac{\partial}{\partial r} \left(\frac{\mu}{r} \frac{\partial u_r}{\partial \theta} + \frac{\mu \partial u_\theta}{\partial r} - \frac{\mu u_\theta}{r} \right) + \frac{1}{r} \frac{\partial}{\partial \theta} \left(\frac{2\mu}{r} \frac{\partial u_\theta}{\partial \theta} + \frac{2\mu u_r}{r} \right) + \frac{\partial}{\partial z} \left(\frac{\mu}{r} \frac{\partial u_z}{\partial \theta} + \frac{\mu \partial u_\theta}{\partial z} \right) - \frac{1}{r} \frac{\partial p}{\partial \theta} + f_\theta, \end{aligned} \quad (S3)$$

where u_r , u_θ , and u_z are the radial velocity, the azimuthal velocity and the axial velocity, respectively. f_θ is the azimuthal interfacial tension. Although the density and viscosity of the dispersed phase (ρ_d and μ_d) and carrier phase (ρ_f and μ_f) are constants, the effective density ρ and the effective viscosity μ are variables in two-phase flow and are defined as $\rho = \alpha\rho_d + (1 - \alpha)\rho_f$ and $\mu = \alpha\mu_d + (1 - \alpha)\mu_f$ in the volume-of-fluid method, where α is the phase fraction of dispersed phase. We apply the following operator to Eq. (S3):

$$\langle \cdot \rangle_{A,t} = \frac{1}{2\pi LT} \int_0^T \int_0^{2\pi} \int_0^L dz d\theta dt, \quad (S4)$$

i.e., we average all the quantities over time, axially, and azimuthally. T is the total time and L is the height of Taylor-Couette system. Given the axial periodicity, azimuthal periodicity, and statistical steady state, any term in Eq. (S3) of the form $\frac{\partial X}{\partial z}$, $\frac{\partial X}{\partial \theta}$, and $\frac{\partial X}{\partial t}$ will be 0 once integrated. The Eq. (S3) is therefore rewritten as

$$\left\langle \frac{2\rho u_r u_\theta}{r} + \frac{\partial(\rho u_r u_\theta)}{\partial r} \right\rangle_{A,t} = \left\langle \frac{2}{r} \left(\frac{\mu}{r} \frac{\partial u_r}{\partial \theta} + \frac{\mu \partial u_\theta}{\partial r} - \frac{\mu u_\theta}{r} \right) + \frac{\partial}{\partial r} \left(\frac{\mu}{r} \frac{\partial u_r}{\partial \theta} + \frac{\mu \partial u_\theta}{\partial r} - \frac{\mu u_\theta}{r} \right) + f_\theta \right\rangle_{A,t}. \quad (S5)$$

Combining the two terms on the left side of Eq. (S5), we have

$$\left\langle \frac{2\rho u_r u_\theta}{r} + \frac{\partial(\rho u_r u_\theta)}{\partial r} \right\rangle_{A,t} = \left\langle \frac{1}{r^2} \left(2r\rho u_r u_\theta + \frac{r^2 \partial(\rho u_r u_\theta)}{\partial r} \right) \right\rangle_{A,t} = \left\langle \frac{1}{r^2} \frac{\partial(r^2 \rho u_r u_\theta)}{\partial r} \right\rangle_{A,t}. \quad (S6)$$

The terms on the right side of Eq. (S5) can be rewritten as

$$\left\langle \frac{2\mu}{r^2} \frac{\partial u_r}{\partial \theta} + \frac{2\mu}{r} \frac{\partial u_\theta}{\partial r} - \frac{2\mu u_\theta}{r^2} - \frac{\mu}{r^2} \frac{\partial u_r}{\partial \theta} + \frac{\mu}{r} \frac{\partial u_r}{\partial r \partial \theta} + \frac{\mu \partial^2 u_\theta}{\partial r^2} + \frac{\mu u_\theta}{r^2} - \frac{\mu}{r} \frac{\partial u_\theta}{\partial r} + \frac{1}{r} \frac{\partial \mu}{\partial r} \frac{\partial u_r}{\partial \theta} + \frac{\partial \mu}{\partial r} \frac{\partial u_\theta}{\partial r} - \frac{\partial \mu}{\partial r} \frac{u_\theta}{r} + f_\theta \right\rangle_{A,t}. \quad (\text{S7})$$

Combining the similar items, including the first and fourth items, the second and eighth items, and the third and seventh items, the Eq. (S7) can be rewritten as

$$\left\langle \frac{\mu}{r^2} \frac{\partial u_r}{\partial \theta} + \frac{\mu}{r} \frac{\partial u_\theta}{\partial r} - \frac{\mu u_\theta}{r^2} + \frac{\mu}{r} \frac{\partial u_r}{\partial r \partial \theta} + \frac{\mu \partial^2 u_\theta}{\partial r^2} + \frac{1}{r} \frac{\partial \mu}{\partial r} \frac{\partial u_r}{\partial \theta} + \frac{\partial \mu}{\partial r} \frac{\partial u_\theta}{\partial r} - \frac{\partial \mu}{\partial r} \frac{u_\theta}{r} + f_\theta \right\rangle_{A,t}. \quad (\text{S8})$$

Combining the second, third, fifth, seventh, and eighth items of Eq. (S8), we have

$$\left\langle \frac{\mu}{r} \frac{\partial u_\theta}{\partial r} - \frac{\mu u_\theta}{r^2} + \frac{\mu \partial^2 u_\theta}{\partial r^2} + \frac{\partial \mu}{\partial r} \frac{\partial u_\theta}{\partial r} - \frac{\partial \mu}{\partial r} \frac{u_\theta}{r} \right\rangle_{A,t} = \left\langle \frac{1}{r^2} \frac{\partial}{\partial r} \left(\mu r^3 \frac{\partial}{\partial r} \left(\frac{u_\theta}{r} \right) \right) \right\rangle_{A,t}. \quad (\text{S9})$$

Combining the remaining items of Eq. (S8), we have

$$\left\langle \frac{\mu}{r^2} \frac{\partial u_r}{\partial \theta} + \frac{\mu}{r} \frac{\partial u_r}{\partial r \partial \theta} + \frac{1}{r} \frac{\partial \mu}{\partial r} \frac{\partial u_r}{\partial \theta} + f_\theta \right\rangle_{A,t} = \left\langle \frac{1}{r^2} \frac{\partial}{\partial r} \left(\mu r \frac{\partial u_r}{\partial \theta} \right) + f_\theta \right\rangle_{A,t}. \quad (\text{S10})$$

We here introduce the operator $\partial_x = \frac{\partial}{\partial x}$ and the angular velocity $\omega = \frac{u_\theta}{r}$. Combining Eq. (S6, S9, S10) and rearranging, we have

$$\left\langle \frac{1}{r^2} \partial_r (r^3 \rho u_r \omega) \right\rangle_{A,t} = \left\langle \frac{1}{r^2} \partial_r (\mu r^3 \partial_r \omega) \right\rangle_{A,t} + \left\langle \frac{1}{r^2} \partial_r (\mu r \partial_\theta u_r) + f_\theta \right\rangle_{A,t}, \quad (\text{S11})$$

$$\langle \partial_r (r^3 \rho u_r \omega) \rangle_{A,t} = \langle \partial_r (\mu r^3 \partial_r \omega) \rangle_{A,t} + \langle \partial_r (\mu r \partial_\theta u_r) + r^2 f_\theta \rangle_{A,t}. \quad (\text{S12})$$

The Eq. (S12) can be rewritten as

$$\partial_r \left(\langle r^3 \rho u_r \omega \rangle_{A,t} - \langle \mu (r^3 \partial_r \omega + r \partial_\theta u_r) \rangle_{A,t} - \int_r \langle r^2 f_\theta \rangle_{A,t} dr \right) = 0, \quad (\text{S13})$$

where the $\int_r \langle r^2 f_\theta \rangle_{A,t} dr$ is the integral of $\langle r^2 f_\theta \rangle_{A,t}$ in the radial direction. We here define $J_{adv}^\omega(r) = \langle r^3 \rho u_r \omega \rangle_{A,t}$, $J_{dif}^\omega(r) = -\langle \mu (r^3 \partial_r \omega + r \partial_\theta u_r) \rangle_{A,t}$, and $J_{int}^\omega(r) = -\int_r \langle r^2 f_\theta \rangle_{A,t} dr$, respectively. We can now integrate the Eq. (S13) from the inner cylinder $r = r_i$ to a generic cylindrical surface $r = r^*$

$$J_{adv}^\omega(r_i) + J_{dif}^\omega(r_i) + J_{int}^\omega(r_i) = J_{adv}^\omega(r^*) + J_{dif}^\omega(r^*) + J_{int}^\omega(r^*). \quad (\text{S14})$$

$J_{adv}^\omega(r_i) = 0$ due to $u_r = 0$ at the inner cylinder, and $J_{int}^\omega(r_i) = 0$ due to $f_\theta = 0$ at the inner cylinder. We can therefore introduce the constant quantity $J^\omega = J_{dif}^\omega(r_i)$ to characterize the transverse current of azimuthal momentum, i.e.,

$$J^\omega = J_{adv}^\omega(r^*) + J_{dif}^\omega(r^*) + J_{int}^\omega(r^*). \quad (\text{S15})$$

The three terms on the right side of Eq. (S15) are the density-related advection contribution, the viscosity-related diffusion contribution, and the interface contribution, respectively. The interface contribution exhibits a distinct form from other two terms, and it is necessary to discuss its physical meaning. For the region between the arbitrary cylindrical surface and the inner cylinder, the interface acts as a source term for momentum transfer. This means that the interface contribution comes from all the interfaces in the region between the cylindrical surface and the inner cylinder. Therefore, it is necessary to sum the influence of all interfaces in the region.

The Eq. (S15) is normalized by the single-phase laminar current $J_{lam}^\omega = 2\mu_f r_i^2 r_o^2 \omega_i / (r_o^2 - r_i^2)$ to obtain the constant Nusselt number $Nu_\omega = J^\omega / J_{lam}^\omega$ and its three contributions related to r including $Nu_{\omega,adv}(r)$, $Nu_{\omega,dif}(r)$, and $Nu_{\omega,int}(r)$, where r_o and ω_i are the radius of outer cylinder and the angular velocity of inner cylinder, respectively. The Nu_ω and T are related by $T = 2\pi L J_{lam}^\omega Nu_\omega$, providing the opportunity to effectively decouple the effects of

density, viscosity, and interface structure on the drag modulation. Figure S3 shows the Nu_ω and its three contributions as a function of the radial position for two-phase flow with $\rho_d = \rho_f/4$ and $\mu_d = \mu_f/4$, and compares them to those for single-phase flow. Given that the value of Nu_ω hardly changes with r , it can be sure that present simulations accurately capture the momentum transfer process. The dispersed phase shows to alter the density-related advection contribution and the viscosity-related diffusion contribution, and induce non-zero interface contribution. By varying density or viscosity of the dispersed phase individually, it becomes possible to reveal their respective roles in drag modulation.

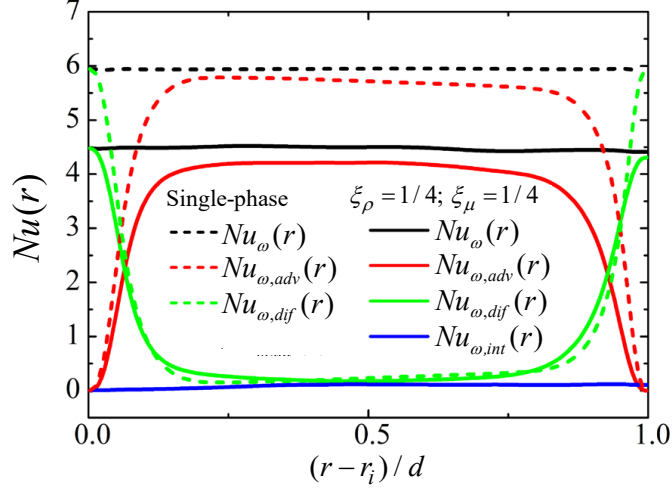


FIG. S3: Momentum transport analysis at $Re = 2000$. The dotted line denotes the single-phase flow and the solid line denotes the two-phase flow with $\varphi = 10\%$.

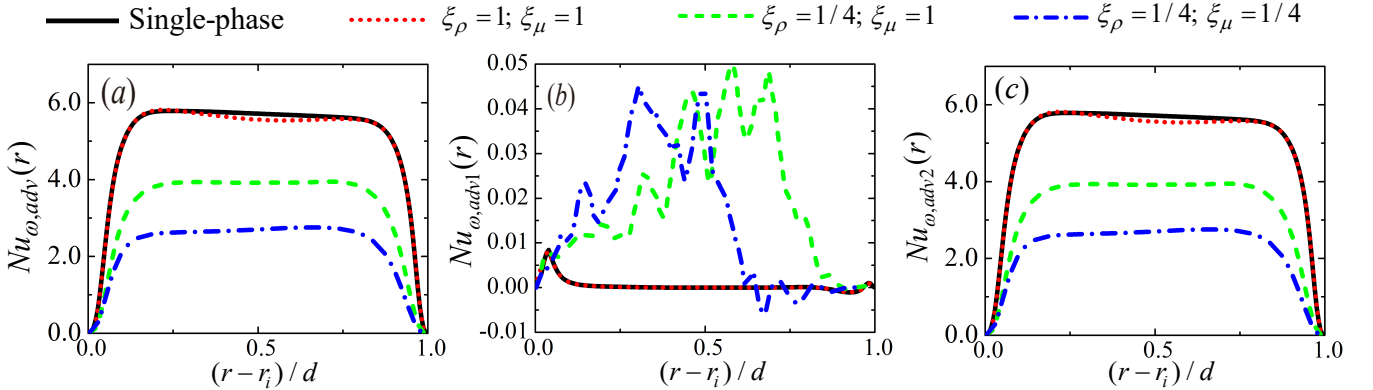


FIG. S4: Advection contribution analysis. (a) The whole advection contribution, (b) the average part, and (c) the turbulent part are shown as a function of the radial position.

Strictly speaking, based on the Favre averaging, the formula of the constant quantity can be rewritten as

$$J^\omega = J_{adv1}^\omega(r) + J_{adv2}^\omega(r) + J_{dif}^\omega(r) + J_{int}^\omega(r), \quad (S16)$$

where $J_{adv1}^\omega(r) = r^2 \widetilde{\rho} \widetilde{u}_r \widetilde{u}_\theta$ and $J_{adv2}^\omega(r) = \langle r^2 \rho u_r'' u_\theta'' \rangle_{A,t}$ are the average part and the turbulent part of the advection term $J_{adv}^\omega(r)$, respectively. Here, $\widetilde{\rho} = \langle \rho \rangle_{A,t}$, $\widetilde{u}_\theta = \langle \rho u_\theta \rangle_{A,t} / \langle \rho \rangle_{A,t}$ and $\widetilde{u}_r = \langle \rho u_r \rangle_{A,t} / \langle \rho \rangle_{A,t}$. The two parts of the advection contribution are normalized to obtain $Nu_{\omega,adv1}(r) = J_{adv1}^\omega(r) / J_{lam}^\omega$ and $Nu_{\omega,adv2}(r) = J_{adv2}^\omega(r) / J_{lam}^\omega$, which are shown in Fig. S4. The average part of the advection contribution is negligible compared to the turbulent part since their maximum ratio is within 1.7% and the mean value of the ratio is about 0.59%. Hence, the advection contribution, the primary focus of our manuscript, is synonymous with the turbulence contribution.

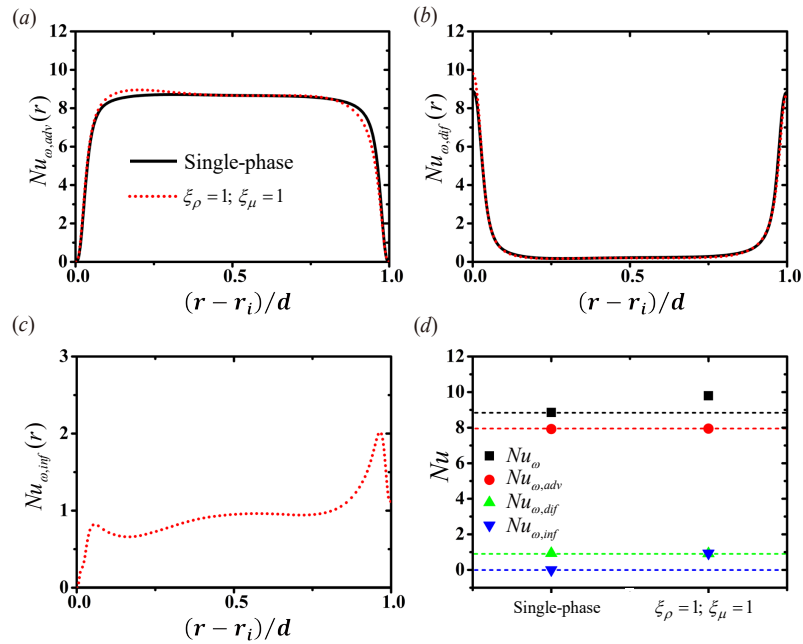


FIG. S5: Momentum transport analysis for $Re = 6000$ and $We = 3915$. (a) The normalized advection contribution, (b) the normalized diffusion contribution, and (c) the normalized interface contribution as a function of the radial position are shown. (d) The momentum transport and its three contributions are averaged in the radial direction. The dashed lines in (d) represent the averaged values for single-phase flow.

Reference

-
- [1] H. G. Weller, *A new approach to VOF-based interface capturing methods for incompressible and compressible flow*, OpenCFD Ltd., Report TR/HGW 4, 35 (2008).
 - [2] K. J. Vachaparambil and K. E. Einarsrud, *Comparison of surface tension models for the volume of fluid method*, Processes 7, 542 (2019).
 - [3] D. J. Harvie, M. Davidson, and M. Rudman, *An analysis of parasitic current generation in volume of fluid simulations*, Applied mathematical modelling 30, 1056 (2006).
 - [4] S. S. Deshpande, L. Anumolu, and M. F. Trujillo, *Evaluating the performance of the two-phase flow solver interFoam*, Computational science & discovery 5, 014016 (2012).
 - [5] F. Xu, P. Zhao, C. Sun, Y. He, and J. Wang, *Direct numerical simulation of Taylor-Couette flow: Regime-dependent role of axial walls*, Chemical Engineering Science 263, 118075 (2022).
 - [6] F. Xu, J. Su, B. Lan, P. Zhao, Y. He, C. Sun, and J. Wang, *Direct numerical simulation of Taylor-Couette flow with vertical asymmetric rough walls*, Journal of Fluid Mechanics 975, A30 (2023).
 - [7] R. Ostilla, R. J. Stevens, S. Grossmann, R. Verzicco, and D. Lohse, *Optimal Taylor-Couette flow: direct numerical simulations*, Journal of fluid mechanics 719, 14 (2013).
 - [8] H. J. Brauckmann and B. Eckhardt, *Direct numerical simulations of local and global torque in Taylor-Couette flow up to $Re = 30\,000$* , Journal of Fluid Mechanics 718, 398 (2013).
 - [9] R. Ostilla-Mónico, R. Verzicco, and D. Lohse, *Effects of the computational domain size on direct numerical simulations of Taylor-Couette turbulence with stationary outer cylinder*, Physics of fluids 27, (2015).